Simultaneous Model Selection and Parameter Estimation for Lithium-Ion Batteries: A Sequential MINLP Solution Approach

Jia-Ni Shen and Yi-Jun He
Dept. of Chemical Engineering, Shanghai Electrochemical Energy Devices Research Center, Shanghai Jiao Tong University, Shanghai 200240, China

Zi-Feng Ma
Dept. of Chemical Engineering, Shanghai Electrochemical Energy Devices Research Center, Shanghai Jiao Tong University, Shanghai 200240, China

Sinopoly Battery Research Center, Shanghai 200241, China

DOI 10.1002/aic.15030
Published online September 21, 2015 in Wiley Online Library (wileyonlinelibrary.com)

Equivalent circuit model (ECM) is a practical and commonly used tool not only in state of charge (SOC) estimation but also in state of health (SOH) monitoring for lithium-ion batteries (LIBs). The functional forms of circuit parameters with respect to SOC in ECM are usually empirical determined, which cannot guarantee to obtain a compact and simple model. A systematical solution framework for simultaneous functional form selection and parameter estimation is proposed. A bi-objective mixed-integer nonlinear programming (MINLP) model is first constructed. Two solution approaches, namely the explicit and implicit methods, are then developed to balance model accuracy and model complexity. The former explicitly treats the model complexity as a constraint and the latter implicitly embeds the model complexity into the objective as a penalty. Both approaches require sequential solution of the transformed MINLP model and an ideal and nadir ideal solutions-based criterion is utilized to terminate the solution procedure for determining the optimal functional forms, in which ideal solution and nadir ideal solution represent the best and worst of each objective, respectively. Both explicit and implicit approaches are thoroughly evaluated and compared through experimental pulse current discharge test and hybrid pulse power characterization test of a commercial LIB. The fitting and prediction results illustrate that the proposed methods can effectively construct an optimal ECM with minimum complexity and prescribed precision requirement. It is thus indicated that the proposed MINLP-based solution framework, which could automatically guide the optimal ECM construction procedure, can be greatly helpful to both SOC estimation and SOH monitoring for LIBs. © 2015 American Institute of Chemical Engineers *AIChE J*, 62: 78–89, 2016
Keywords: lithium-ion batteries, state of charge, equivalent circuit model, functional forms selection, parameter estimation, mixed-integer nonlinear programming

Introduction

Lithium-ion batteries (LIBs), with high energy density, high operating voltage levels, and long cycle life, are increasingly used as the energy storage and power source for various electrical systems, such as hybrid electric vehicles, renewable power systems, and portable electronic devices.[1–3] Although the research on positive and negative electrodes, separator and electrolyte performance as well as manufacture technology have made steady progress, how to guarantee the safe, reliable, and efficient operation of LIBs still remains a challenging task. This challenge demands a properly designed smart battery management system (BMS) for protecting the battery from unsafe operating region, performing accurate state of charge (SOC) estimation and state of health (SOH) prognostics, implementing thermal management, controlling charge rate, and so on.[4–6] As a high-fidelity BMS relies on an accurate battery model, it is important to establish an accurate relationship between the nonlinear battery behavior and many factors, such as SOC, aging, temperature, and operating conditions.[7] In the past decade, various modeling approaches with different complexity have been proposed to describe the complex dynamic behaviors of LIBs and can be broadly classified into three categories: electrochemical model,[8] equivalent circuit model (ECM),[9–11] and data-driven model.[12,13] In comparison to electrochemical and data-driven models, ECM has attracted plenty of attention in the BMS community, as it is fast to execute, simple, and intuitive to analyze, and can be easily integrated with control algorithms for performing SOC estimation and SOH monitoring.

ECMs describe the battery behaviors using capacitors, voltage and current sources, and resistors from the point of view of circuit analysis. They can be mainly divided into two types: impedance-based[11,14–16] and Thevenin-based models.[9,10,17–19]

Correspondence concerning this article should be addressed to Y.-J. He at heyijun@sjtu.edu.cn.

The former is modeled by means of electrochemical impedance spectroscopy (EIS), while the latter is modeled by means of current-voltage (I-V) curves. Although EIS can provide more detailed kinetic information of LIBs than traditional I-V test, it is costly and time-consuming, which hinders the online application of impedance-based models in the BMS. Conversely, as voltage and current sensors are commonly cheaply deployed in the BMS, the Thevenin-based models, being capable of capturing complex I-V characteristics, have been widely used in SOC estimation, runtime prediction, peak power estimation, and so forth. The commonly used Thevenin-based model is a circuit with a controlled voltage source in series with resistor and resistance-capacitance (RC) parallel networks. A voltage-controlled voltage source is used to simulate the open circuit voltage (OCV). A resistor models the internal ohmic resistance of the battery, whereas the RC networks take into account the transient response characteristic associated with the electrochemical process. To improve battery design and control algorithms, the nonlinear effects of different factors, such as SOC,[20–22] temperature,[22–24] C-rate,[15,18,23] cycle number,[23] and current direction,[23,24] on the circuit parameters have been extensively investigated. Moreover, some fundamental issues, that is, model structure selection and parameter estimation method, have been explored. Although the model structure includes both the number of RC parallel networks and the functional forms of the circuit parameters, recent studies have mostly focused on evaluating the effect of the number of RC networks on the accuracy and computational efficiency of ECMs,[18,21,25,26] the effect of the functional forms of circuit parameters is often ignored and needs to be further explored. Moreover, optimal selection of model structure is scarcely investigated.

The relationship between circuit parameters and nonlinear effects can be described either by model-free look-up table[10,19,21,26,27] or analytical expression.[9,18,22] Look-up table approach is visual and intuitive, but it is often memory intensive and inaccurate to some extent when used in real-world applications. Analytical expression approach based on parameterization is flexible and computationally efficient, and thus it is more easily employed in real-time simulation. There are usually two consecutive steps in the analytical expression approach: functional form determination and parameter estimation. In previous works, functional form is usually empirical selected in terms of fitting accuracy, without explicitly accounting for the computational complexity. Generally, model accuracy and model complexity are often conflicting. That means, improving the model accuracy often increases the model complexity, which results in higher computational complexity. In fact, most of applications, particular real-time control system and on-line SOC estimation, require the model not only being accurate enough to model the battery behaviors but also being simple enough to run on an embedded controller.[7] Therefore, a thorough understanding of the relationship between model accuracy and model complexity is of vital importance for establishing a practical effective ECM. In this study, we propose a systematical solution framework for simultaneous functional form selection and parameter estimation. To establish the ECM with minimum complexity, both explicit and implicit approaches are developed, in which mixed-integer nonlinear programming (MINLP) problems are sequentially and efficiently solved by BARON.[28] Moreover, an ideal and nadir ideal solutions-based criterion has been utilized to terminate the solution procedure for determining the optimal functional forms. To the best of our knowledge, this study is the first attempt to provide an optimization-based approach for balancing model accuracy and model complexity in the modeling of LIBs.

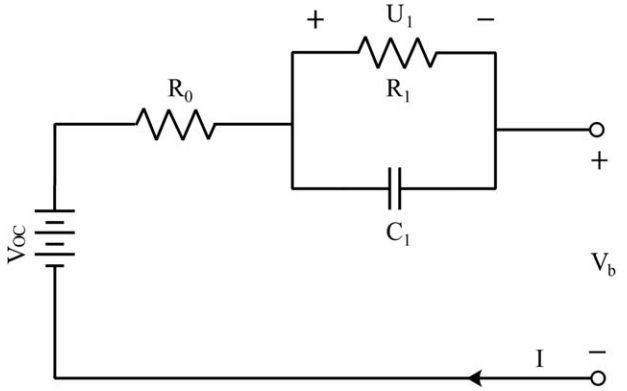

Figure 1. First-order Thevenin-based model of LIBs.

The remainder of this article is structured as follows. The problem of functional form selection of circuit parameters in ECM is first described. Then, two MINLP models for explicit and implicit approaches and a criterion for model selection are proposed. The effectiveness of the proposed methods is next validated by the experimental datasets. Finally, conclusions are presented.

Methodology

First-order Thevenin-based model

For the description of the nonlinear dynamic behaviors of charging/discharging and voltage relaxation processes in LIBs, a first-order Thevenin-based model shown in Figure 1 is employed. As shown in Figure 1, it mainly consists of three parts, including an OCV V_{OC}, an ohmic resistance R_0, and a parallel RC network. The RC network includes a polarization resistance R_1 and an equivalent capacitance C_1. The equivalent capacitance is used to describe the transient response during charging and discharging. V_1 is the voltage across the capacitance C_1, V_b is the terminal voltage, and I is load current with a positive value at discharging and a negative value at charge. Although all circuit parameters (e.g., V_{OC}, R_0, R_1, and C_1) are usually dependent on SOC and temperature, this study only focuses on establishing analytical expressions between circuit parameters and SOC for validating the effectiveness of the proposed simultaneous model structure selection and parameter estimation method. In addition, as the OCV shows an increasing monotonicity with respect to SOC, a monotone polynomial OCV model developed in our previous work is used.[29]

SOC over time t is calculated by Coulomb counting

$$\mathrm{SOC}(t)=\mathrm{SOC}(0)+\frac{1}{C}\int_0^t I(\tau)d\tau \tag{1}$$

where SOC(0) is the initial value of SOC and C is the nominal capacity of battery. As current and voltage are often measured at discrete time with a specific sampling frequency, the integration of the right-hand second term of Eq. 1 can be easily calculated by summation and then Eq. 1 is reformulated as

$$\mathrm{SOC}(t_K)=\mathrm{SOC}(t_0)+\frac{1}{C}\sum_{k=1}^{K} I(t_{k-1})\Delta t \tag{2}$$

where $\Delta t=t_k-t_{k-1}$ is the time interval between two sampling points, and $I(t_{k-1})$ denotes the measured current at time t_{k-1} and is assumed to be constant at the time interval $[t_{k-1}, t_k]$. K is the number of sampling points.

Based on Kirchhoff's current law, the relationship between the currents can be described as

$$I=I_1+I_2 \tag{3}$$

where current I_1 and current I_2 go through resistance R_1 and capacitance C_1, respectively.

The relationship between the charge Q_1, voltage V_1, and current I_1 in the capacitance can be described as

$$I_1=\frac{dQ_1}{dt}=\frac{dC_1V_1}{dt}=C_1\frac{dV_1}{dt} \tag{4}$$

The current I_2 related to V_1 is given by

$$I_2=\frac{V_1}{R_1} \tag{5}$$

The relationship between the terminal voltage, OCV, voltage drop through the ohmic resistance, and voltage across the capacitance is described as

$$V_b=V_{\mathrm{OC}}-IR_0-V_1 \tag{6}$$

Hence, the nonlinear charging/discharging dynamics of the LIBs can be described by Eqs. 3–6. To perform parameter estimation efficiently, the analytical solution of the above ECM is calculated. At the time interval $[t_{k-1}, t_k]$, it is reasonable to assume that four circuit parameters, that is, V_{OC}, R_0, R_1, and C_1, keep constant and they are denoted as $V_{\mathrm{OC}}(t_{k-1})$, $R_0(t_{k-1})$, $R_1(t_{k-1})$, and $C_1(t_{k-1})$, respectively. Let $\tau(t_{k-1})=R_1(t_{k-1})C_1(t_{k-1})$ denote the time constant of the parallel RC network during the time interval $[t_{k-1}, t_k]$. At discrete time t_k, the voltage $V_1(t_k)$ can be analytically derived from Eqs. 3–5 and described as

$$\begin{aligned} V_1(t_k)=&V_1(t_{k-1})\exp\left(-\frac{\Delta t}{\tau(t_{k-1})}\right)\\ &+I(t_{k-1})R_1(t_{k-1})\left[1-\exp\left(-\frac{\Delta t}{\tau(t_{k-1})}\right)\right] \end{aligned} \tag{7}$$

Then, based on Eq. 6, the terminal voltage $\hat{V}_b(t_k)$ at discrete time t_k can be calculated as

$$\hat{V}_b(t_k)=V_{OC}(t_k)-I(t_k)R_0(t_k)-V_1(t_k) \tag{8}$$

Note that although the above circuit parameters are represented as functions of time, they are indeed dependent on SOC and can be further precisely represented as $V_{\mathrm{OC}}(\mathrm{SOC}(t_{k-1}))$, $R_0(\mathrm{SOC}(t_{k-1}))$, $R_1(\mathrm{SOC}(t_{k-1}))$, and $C_1(\mathrm{SOC}(t_{k-1}))$. Generally, at a specific SOC, those parameters can be determined using a voltage response profile during a rest period, in which the ohmic resistance R_0 is directly determined by the ratio of the initial voltage change to the charging/discharging current, and the polarization resistance R_1 and equivalent capacitance C_1 are usually determined using least squares methods. The above procedures will be repeatedly implemented for other SOC points, and then a look-up table could be constructed for each circuit parameter. Then, the interpolation method is applied to estimate the circuit parameter values at other unseen SOC points. However, construction of the look-up tables would take higher computational cost, as it needs to implement numerous parameter estimation procedures. Furthermore, the interpolation method cannot guarantee to capture the true relationship between the circuit parameters and SOC, which might results in poor prediction performance. More importantly, the interpolation method is often less efficient than analytical models in the case of real-time application.

Bi-objective MINLP model

In this study, analytical expression method is used to model the relationship between the circuit parameters and SOC, which is greatly helpful toward real-time application. There have been various function types used to model the relationship between the circuit parameters and SOC, including polynomial,[19] exponential,[9,30] and combination forms.[18] Based on an overall consideration of function complexity and computational efficiency, polynomial function type is the commonly used one. However, it is noticed that most of studies select a same complete form of polynomials for all circuit parameters in an empirical way, which might result in an overestimation of the suitable function complexity and higher computational cost. Generally, with the increasing of polynomial functional form complexity, the fitting ability of the model could be improved, but the computational cost becomes higher. It implies that balancing the trade-off between model accuracy and complexity is significantly important to meet the real-time application requirement.

Therefore, this study will focus on applying polynomial functions to model the relationship between the circuit parameters and SOC, and proposing a bi-objective optimization problem for simultaneously maximizing model accuracy and minimizing model complexity. It should be noted that the model complexity minimization calls for optimal selection of the proper functional form, which often result in a MINLP problem. The bi-objective MINLP model **(P0)** for constructing the ECM of LIBs is formulated as

$$\min \mathrm{SSE}=\sum_{k=1}^{K}\left[\hat{V}_b(t_k)-V_b(t_k)\right]^2 \tag{9}$$

$$\min \mathrm{MC}=\sum_{i=1}^{3}\sum_{j=1}^{N} y_{ij} \tag{10}$$

s.t.

Constraints (7) and (8)

$$\mathrm{SOC}(t_k)=\mathrm{SOC}(t_{k-1})+\frac{I(t_{k-1})\Delta t}{C}, k=1,\cdots,K \tag{11}$$

$$R_0(\mathrm{SOC}(t_{k-1}))=\sum_{j=0}^{N} y_{1j}\beta_{1j}\mathrm{SOC}(t_{k-1})^j, k=1,\cdots,K \tag{12}$$

$$R_1(\mathrm{SOC}(t_{k-1}))=\sum_{j=0}^{N} y_{2j}\beta_{2j}\mathrm{SOC}(t_{k-1})^j, k=1,\cdots,K \tag{13}$$

$$C_1(\mathrm{SOC}(t_{k-1}))=\sum_{j=0}^{N} y_{3j}\beta_{3j}\mathrm{SOC}(t_{k-1})^j, k=1,\cdots,K \tag{14}$$

$$\sum_{j=0}^{N} y_{ij}\beta_{ij}\mathrm{SOC}(t_{k-1})^j > 0, \forall i \tag{15}$$

$$\sum_{j=1}^{N} y_{ij} \geq 1, \forall i \tag{16}$$

$$y_{ij}=\{0,1\}, i=1,2,3;\ j=1,\cdots,N \tag{17}$$

$$\beta_{ij}^{\mathrm{L}} \leq \beta_{ij} \leq \beta_{ij}^{\mathrm{U}}, i=1,2,3;\ j=1,\cdots,N \tag{18}$$

The first objective function SSE shown in Eq. 9 denotes the sum of the squared error (SSE) between the fitted terminal voltage $\hat{V}_b$ and measured terminal voltage V_b, and the second objective function MC shown in Eq. 10, representing the model complexity, is the total selected number of polynomial terms for three circuit parameters. Equations 12–14 show the polynomial functions of the ohmic resistance, polarization resistance, and equivalent capacitance, respectively. Binary variables y_{ij} is 1 if the jth term in the ith polynomial function is selected. β_{ij}^{L} and β_{ij}^{U} are the lower and upper bounds of polynomial coefficient β_{ij}. There are total $6(N+1)$ binary and continuous variables to be optimized. The constraint in Eq. 15 ensures each circuit parameter to be always positive. The constraint in Eq. 16 denotes that there exists at least one term for each circuit parameter, which is applied to guarantee the existence of the ohmic resistance, polarization resistance, and equivalent capacitance in the constructed ECM of LIBs.

As most of global solvers cannot be directly applied to tackle bi-objective MINLP model **P0**, the explicit and implicit solution strategies are proposed. Both explicit and implicit solution strategies need to sequentially solve a single objective MINLP model, where the former explicitly treats the model complexity index MC as an equality constraint and the latter implicitly added l_1 penalty on coefficients into the SSE objective function. The details of the explicit and implicit approaches are described in the following two sections.

Explicit solution approach

In explicit solution approach, a single-objective MINLP model is sequentially solved through successive increment of the model complexity, in which the model complexity is treated as an equality constraint and the objective function SSE is minimized. Based on Eq. 16, the minimum of MC is 3 and consequently the value of MC can increase from 3 to $3(N+1)$ step by step. In the worst case, there are total $3N+1$ sequential MINLP models to be solved. However, in the most cases, only several MINLP models need to be solved in terms of a prescribed stopping criterion. To improve the solution efficiency, the bilinear terms $y_{ij}\beta_{ij}$ in Eqs. 12–15 are replaced with β_{ij} and the following constraints

$$y_{ij}\beta_{ij}^{\mathrm{L}} \leq \beta_{ij} \leq y_{ij}\beta_{ij}^{\mathrm{U}},\ i=1,2,3;\ j=1,\cdots,N \tag{19}$$

The above equation ensure that if y_{ij} is zero, β_{ij} should be exactly zero; if y_{ij} is one, β_{ij} is allowed to take a nonzero value within its lower and upper bounds. Thus, the sequential single objective MINLP model (**P1**) can be formulated as

$$\min \mathrm{SSE}=\sum_{k=1}^{K}\left[\hat{V}_b(t_k)-V_b(t_k)\right]^2 \tag{20}$$

s.t.

Constraints (7), (8), (11), (16), (17), and (19)

$$\mathrm{MC}=\sum_{i=1}^{3}\sum_{j=1}^{N} y_{ij} \tag{21}$$

$$R_0(\mathrm{SOC}(t_{k-1}))=\sum_{j=0}^{N}\beta_{1j}\mathrm{SOC}(t_{k-1})^j, k=1,\cdots,K \tag{22}$$

$$R_1(\mathrm{SOC}(t_{k-1}))=\sum_{j=0}^{N}\beta_{2j}\mathrm{SOC}(t_{k-1})^j, k=1,\cdots,K \tag{23}$$

$$C_1(\mathrm{SOC}(t_{k-1}))=\sum_{j=0}^{N}\beta_{3j}\mathrm{SOC}(t_{k-1})^j, k=1,\cdots,K \tag{24}$$

$$\sum_{j=0}^{N}\beta_{ij}\mathrm{SOC}(t_{k-1})^j > 0, \forall i \tag{25}$$

Implicit solution approach

Unlike explicit solution approach, implicit solution approach replaces the explicit model complexity constraint with an implicit l_1 norm penalty on polynomial coefficients. The l_1-penalized objective function is formulated as

$$\min \sum_{k=1}^{K}\left[\hat{V}_b(t_k)-V_b(t_k)\right]^2+\sum_{i=1}^{3}\lambda_i\|\boldsymbol{\beta}_i\|_1 \tag{26}$$

where $\lambda_i \geq 0$, $i=1,2,3$ are the regularization parameters, and $\|\boldsymbol{\beta}_i\|_1=\sum_{j=0}^{N}|\beta_{ij}|$ denotes the l_1 norm of a vector $\boldsymbol{\beta}_i$. Generally, with the increasing of penalties λ_i, the fitting error increases and the polynomial coefficients are shrunk toward zeros. If the regularization values are sufficiently large, some coefficients can be exactly zero, giving rise to model size reduction and the functional form selection. As the values of the ohmic resistance, polarization resistance and equivalent capacitance usually have different orders, different regularization values should be applied. It has been recognized that the values of ohmic resistance and polarization resistance usually have almost the same order, while the ratio of ohmic (or polarization) resistance to equivalent capacitance is about 10^{-6}.[27,31] Hence, in this study, the regularization values of λ_2 and λ_3 are simply set equal to λ_1 and $10^{-6}\lambda_1$, respectively, and consequently a single regularization parameter λ can be applied.

As l_1 norm penalty is nonlinear and cannot be directly handled by the global solver, a new continuous variable α_{ij} and a binary variable y_{ij} are introduced to replace the absolute value of β_{ij} with a set of additional constraints. Let y_{ij} denote the indication of the sign of β_{ij}, where y_{ij} is one if $\beta_{ij} \geq 0$, and y_{ij} is zero if $\beta_{ij} \leq 0$. Then, the disjunctions in terms of y_{ij} with respect to α_{ij} and β_{ij} can be expressed as

$$\begin{bmatrix} y_{ij}=1 \\ \beta_{ij} \geq 0 \\ \alpha_{ij}=\beta_{ij} \end{bmatrix} \vee \begin{bmatrix} y_{ij}=0 \\ \beta_{ij} \leq 0 \\ \alpha_{ij}=-\beta_{ij} \end{bmatrix}, \forall i,j \tag{27}$$

The above disjunction term can be further converted into the following constraints based on big-M method

$$-M(1-y_{ij}) \leq \alpha_{ij}-\beta_{ij} \leq M(1-y_{ij}), \forall i,j \tag{28}$$

$$-My_{ij} \leq \alpha_{ij}+\beta_{ij} \leq My_{ij}, \forall i,j \tag{29}$$

$$\beta_{ij} \geq -M(1-y_{ij}), \forall i,j \tag{30}$$

$$\beta_{ij} \le My_{ij}, \forall i,j \tag{31}$$

As it is easy to obtain $\alpha_{ij} \ge \beta_{ij}$ and $\alpha_{ij} \ge -\beta_{ij}$, Eqs. 28 and 29 can be further tightened as

$$0 \le \alpha_{ij} - \beta_{ij} \le M(1-y_{ij}), \forall i,j \tag{32}$$

$$0 \le \alpha_{ij} + \beta_{ij} \le My_{ij}, \forall i,j \tag{33}$$

Hence, the MINLP model (**P2**) of the implicit solution approach can be given as

$$\min \sum_{k=1}^{K} \left[\hat{V}_b(t_k) - V_b(t_k)\right]^2 + \lambda \left[\sum_{j=0}^{N} \alpha_{1j} + \sum_{j=0}^{N} \alpha_{2j} + 10^{-7} \sum_{j=0}^{N} \alpha_{3j}\right] \tag{34}$$

s.t.

Constraints (7), (8), (11), (17), (18), (22)–(25), and (30)–(33)

Implementation framework of explicit and implicit solution approaches

The implementation flowchart of the explicit and implicit approaches is shown in Figure 2. The MINLP model **P1** or **P2** is iteratively solved using BARON until the stopping criteria are met. In the explicit approach, the value of MC increases from 3 to $3(N+1)$, while in the implicit approach, the value of regularization parameter λ is set to be logarithmic decrease. Note that with the increasing of MC or the decreasing of λ, both fitting accuracy and optimal selected polynomial terms will usually increase.

To evaluate the fitting and prediction performance of the established model, two criteria, namely the root mean square error (RMSE) and mean absolute percentage error (MAPE), are commonly used, which are defined as Eqs. 35 and 36, respectively

$$\text{RMSE} = \sqrt{\frac{\sum_{k=1}^{K} \left(\hat{V}_b(t_k) - V_b(t_k)\right)^2}{K}} \tag{35}$$

$$\text{MAPE}(\%) = \frac{100}{K} \sum_{k=1}^{K} \left| \frac{\hat{V}_b(t_k) - V_b(t_k)}{V_b(t_k)} \right| \tag{36}$$

There are two types of stopping criteria applied in the proposed solution framework. First, the maximal allowable fitting error of RMSE_{mx} or MAPE_{mx} is set to ensure the constructed model can satisfy the practical precision requirement. The values of RMSE_{mx} and MAPE_{mx} are simply set equal to 10 mV and 0.25%, respectively, in this study. Then, a weighted distance criterion based on ideal and nadir ideal solutions is introduced to evaluate the solution quality in terms of two conflicting objective, that is, the model complexity and fitting error.

Smaller values of MC and RMSE indicate the better quality of a solution. The ideal and nadir ideal solution are represented as $[\text{MC}_{\text{min}}, \text{RMSE}_{\text{min}}]$ and $[\text{MC}_{\text{max}}, \text{RMSE}_{\text{max}}]$, respectively. In the explicit approach, the value of MC_{min} is set to 3 and the value of RMSE_{max} is obtained by solving the MINLP model **P1** with the MC of 3. In the implicit approach, the values of MC_{min} and RMSE_{max} can be obtained by solving the MINLP model **P2** with the initial regularization parameter λ_0. For both explicit and implicit approaches, the value of MC_{max} and RMSE_{min} are simply set to $3(N+1)$ and 0 mV, respectively. In general, the best solution should not only have the shortest distance from the ideal solution, but also have the longest distance from the nadir ideal solution. Thus, a criterion C is defined to characterize the preferable of the solution [MC, RMSE]

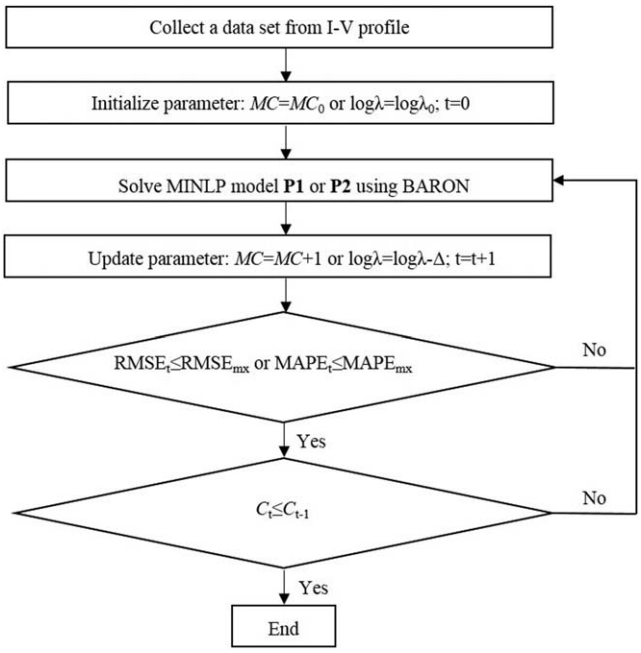

Figure 2. A flowchart of the explicit and implicit solution approaches.

$$C = \frac{d^-}{d^+ + d^-} \tag{37}$$

where d^+ and d^-, shown in Eqs. 38 and 39, denotes the normalized distance between the solution and ideal solution and the distance between the solution and nadir ideal solution, respectively

$$d^+ = \sqrt{(\text{MC}_{\text{norm}})^2 + (\text{RMSE}_{\text{norm}})^2} \tag{38}$$

$$d^- = \sqrt{(\text{MC}_{\text{norm}} - 1)^2 + (\text{RMSE}_{\text{norm}} - 1)^2} \tag{39}$$

where MC_{norm} and $\text{RMSE}_{\text{norm}}$ are normalized values of MC and RMSE based on ideal and nadir ideal solutions, respectively

$$\text{MC}_{\text{norm}} = \frac{\text{MC} - \text{MC}_{\text{min}}}{\text{MC}_{\text{max}} - \text{MC}_{\text{min}}} \tag{40}$$

$$\text{RMSE}_{\text{norm}} = \frac{\text{RMSE} - \text{RMSE}_{\text{min}}}{\text{RMSE}_{\text{max}} - \text{RMSE}_{\text{min}}} \tag{41}$$

Note that based on normalization, the ideal and nadir solutions can be simply represented as [0, 0] and [1, 1], respectively.

Experimental

A commercial HEADWAY D38120 LiFePO_4 battery cell with nominal capacity of 8 Ah and nominal voltage of 3.2 V was used to test the battery charging/discharging behaviors, which were conducted with a NEWARE CT-3002-5V500A battery test system and a HARDY HLT4005P programmable temperature test chamber. The data acquisition system has a

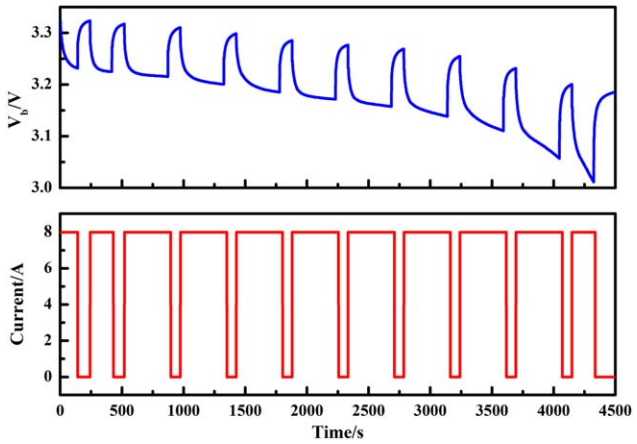

Figure 3. Typical voltage response curve in pulse discharge current condition.

[Color figure can be viewed in the online issue, which is available at wileyonlinelibrary.com.]

logging frequency of 1 Hz, and the measurement precision of both current and voltage is 0.05%. After raising or lowering the cell ambient temperature to the target value, the battery rested for 5 h to achieve thermal equalization. The battery was first charged to its full capacity through constant current constant voltage, and then rested for 2 h. Then, two characteristic tests were performed for parameter identification and model validation, that is, predefined pulse current discharge (PCD) test and hybrid pulse power characterization (HPPC) test. To avoid over discharge, we only test the characteristic of LIB in the SOC range from 100 to 5%.

The PCD test consists of a sequence of constant current discharge and rest periods. Figure 3 shows a typical voltage response curve during a complete PCD test, where the battery was discharged at 1C rate (8A) for 180 s to reduce 5% of the battery's SOC during the first two current pulses, and discharged at 1C rate for 360 s to reduce 10% of the battery's SOC during subsequent current pulses. Between the discharge periods, the battery is rested for 100 s to produce the voltage relaxation. This discharge-rest profile was repeatedly conducted until the end of discharge. It could be seen that the battery voltage response curve shows a nonlinear dynamic characteristic in both discharge and rest periods.

The HPPC test is from FreedomCAR Battery Test Manual for Power-Assist Hybrid Electric Vehicles.[32] In this HPPC profile, the battery was discharged at 2.5C rate (20A) for 10 s, rested at zero current for 40 s, and subsequently charged at 2C rate (16A) for 10 s. Figure 4 shows a typical voltage response curve during a complete HPPC test. The battery was first discharged at 1C rate for 180 s to reduce 10% of the battery's SOC and then rested for 100 s. Subsequently, single repetitions of HPPC profile as described was conducted, separated by 10% SOC constant current 1C rate discharge segments, each followed by a 100 s rest period. Similarly, it could be seen that the voltage response curve shows a nonlinear dynamic characteristic for each period, that is, charge, discharge, and rest.

Results and Discussion

The datasets collected from PCD test under 298, 313, and 333 K are used for model construction and the dataset from HPPC test at 313 K is used for model prediction performance validation. Both explicit and implicit approaches are implemented and solved in GAMS 24.4.0 and a branch and reduce algorithm based solver BARON 14.4.0 is used to solve MINLP models **P1** and **P2**. All computations are carried out on a PC with 2.40 GHz processor and 8 GB of RAM. Both the absolute and relative tolerances are set to 0.001, and the maximum CPU time is set to 50,000 s in all calculations. A maximal polynomial order of 5 is set for all computation.

Model validation using the explicit solution approach

The explicit solution approach is first used to construct the ECM model using PCD test at different temperatures. The MINLP models **P1** are sequentially solved for all possible MCs, namely from 3 to 18, to examine the effect of model complexity on the fitting performance. Figures 5a, b show the fitting RMSE and MAPE with respect to MC at different temperatures, respectively. As shown in Figure 5a, the RMSE at low temperature is larger than that at high temperature for the same MC. The possible reason is that voltage response curves at low temperature usually exhibit sharper changes than that at high temperature, which would make the model difficult to capture the battery behavior. The RMSE value first decreases sharply with the increasing of MC and then keeps constant when the value of MC is above 9 at three temperatures. For example, at the temperature of 298 K, the RMSE value significantly decreases from 15.4 to 7.8 mV when the value of MC increases from 3 to 6 and are less than 7 mV as the value of MC above 8. It implies that the fitting accuracy can be usually improved with the increasing of the model complexity. However, note that a highly complex model often require high computational cost and will increase the over-fitting risk. Hence, it is important to balance the trade-off between the model complexity and fitting accuracy to obtain a satisfactory model. From Figure 5a, it can be also found that the RMSE curves have the MC turning points of 6, 5, and 4 at the temperatures of 298, 313, and 333 K, respectively. That means, a relatively complex model is often required to capture the nonlinear voltage response behaviors at low temperature. For the temperatures of 298, 313, and 333 K, the minimum values of RMSE are about 6.4, 5.5, and 4.3 mV, respectively. The fitting MAPE in Figure 5b shows a similar result as Figure 5a. The minimum values of MAPE are 0.16%, 0.14% and 0.10% at the temperatures of 298, 313, and 333 K, respectively.

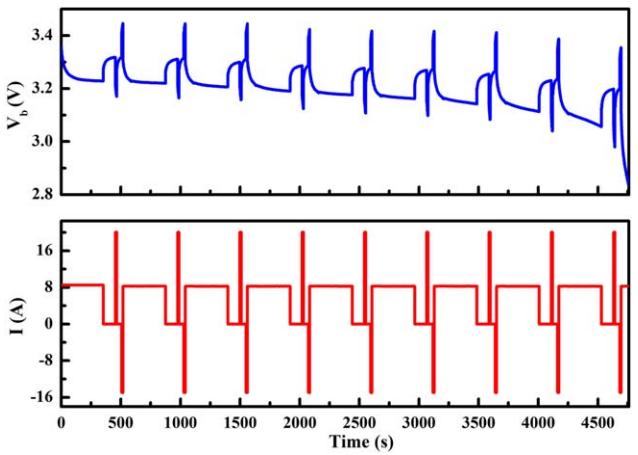

Figure 4. Typical voltage response curve in HPPC test.

[Color figure can be viewed in the online issue, which is available at wileyonlinelibrary.com.]

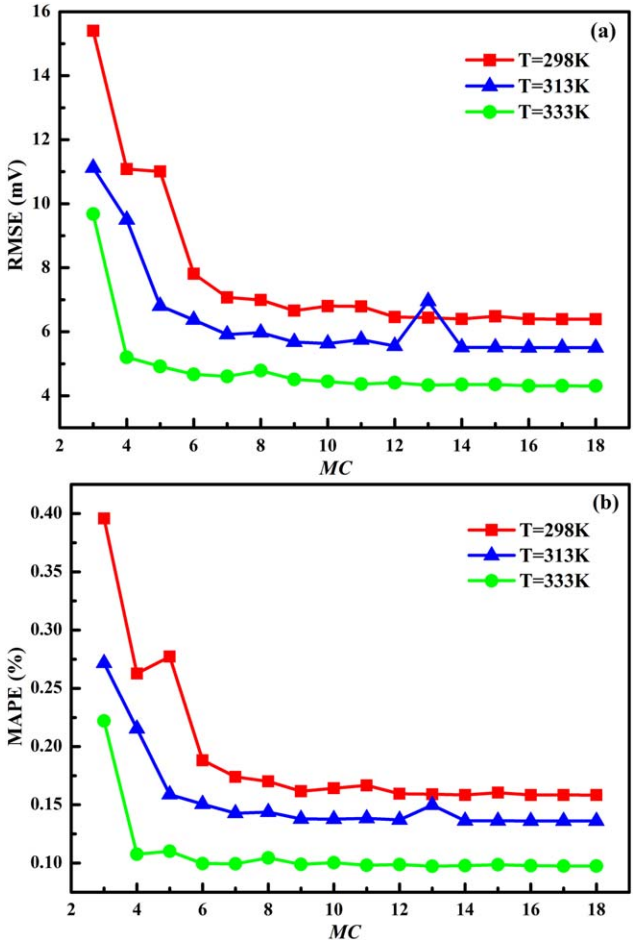

Figure 5. Model fitting performance with respect to MC at different temperatures in PCD condition using the explicit solution approach: (a) RMSE; (b) MAPE.

[Color figure can be viewed in the online issue, which is available at wileyonlinelibrary.com.]

Figures 5a, b, therefore, indicate that the performance of a complete polynomial model can be achieved with a relatively simple model by means of the solution of MINLP model. In addition, it should be pointed the reason for the existence of abnormal point of thirteen-term model at 313 K is that the global optimization ability of current BARON is not enough to tackle with this complex MINLP problem. To illustrate this point, we formulate the MINLP model with MC = 13 by appending a term to the optimal functional form of twelve-term model, it was found the accuracy of thirteen-term model is slightly higher than that of twelve-term model, and is quite close to that of fourteen-term model. Based on our computation experiments, it is also found that 60,000 s is long enough to obtain optimal MINLP solutions and only several thousand seconds are needed for obtain satisfactory solutions in most cases.

To balance the trade-off between the model accuracy and complexity, the criterion C is calculated based on Eq. 37 in term of the result of Figure 5a. Figure 6 plots the criterion C with respect to MC at 298, 313, and 333 K, respectively. It is observed that with the increasing of MC, the value of C usually first increases and then decreases for these three temperatures. Based on the definition of the criterion C, a larger value of C often indicates a better solution in the viewpoint of the compromise of two conflict objectives, that is, model accuracy and complexity. For all temperatures, it is also found that the maximum value of C is achieved with the MC value of 6. Thus, through integrated consideration of the results in Figures 5 and 6, a multicriterion optimal decision can be made, in which a model with six terms can be selected by balancing the model accuracy and complexity. Note that although the same number of terms is selected for different temperatures, the functional forms of circuit parameters might be significantly different.

Figure 7 compares the fitting results of battery voltage responses using the best three-, six-, and eighteen-term models determined in PCD test at 313 K. As shown in Figure 7a, the fitting battery voltage responses obtained from the three-term model poorly match the measured data at the whole SOC range, especially at the SOC range of 30–80%. The RMSE and MAPE of the three-term model are 11.12 mV and 0.27%, respectively. Moreover, it is found that the three-term model underestimates the terminal voltages at the normal operating SOC range of 30–80%, which would result in a significant model error under the continuous discharge conditions and consequently reduce the energy utilization efficiency. The fitting battery voltage responses obtained from the six-term model are almost the same to those from the eighteen-term model, and match very well with the measured data over the entire SOC range. The RMSE values of the six- and eighteen-term models are only 6.36 and 5.50 mV, respectively, and the MAPE values of them are 0.15% and 0.14%, respectively. Figure 7b shows the enlarged section of fitting results at the 60–70% SOC. It can be clearly seen that the three-term model almost shows a linear decreasing relationship of voltage response with respect to time and fails to capture the nonlinear behavior in both discharge and rest periods. Conversely, both six- and eighteen-term models could perfectly capture the nonlinear voltage response in the discharge period and exhibit a relatively small overestimation of terminal voltage in the rest period. The possible reason is that the one RC network cannot exactly capture the nonlinear dynamic changes of voltage during the rest period. Generally, the fitting accuracy of the rest period can be further improve by employing more RC networks, however, the accuracy gained seems too small

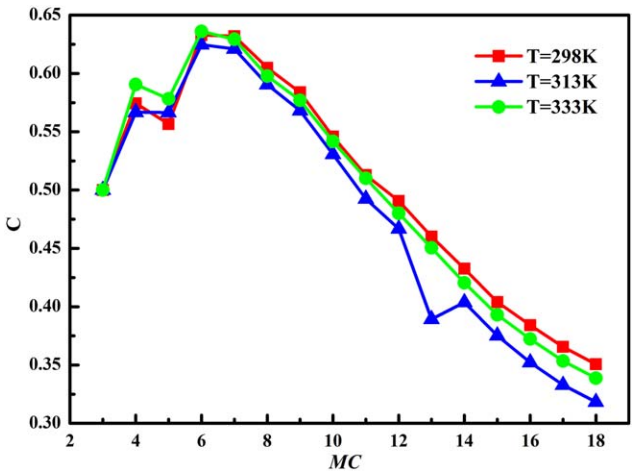

Figure 6. Criterion of model with different MC under different temperatures in PCD condition using the explicit solution approach.

[Color figure can be viewed in the online issue, which is available at wileyonlinelibrary.com.]

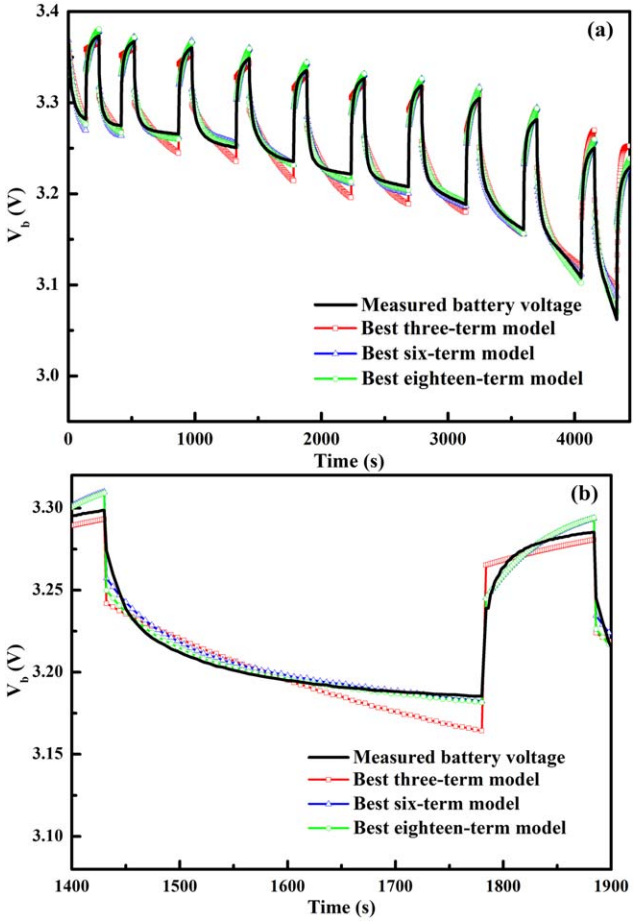

Figure 7. Comparison of fitting results of battery voltage responses using the best three-, six-, and eighteen-term models in PCD test at 313 K: (a) 0–100% SOC; (b) 60–70% SOC.

[Color figure can be viewed in the online issue, which is available at wileyonlinelibrary.com.]

compared to the increased complexity. In a word, the fitting results demonstrate that the best model derived from explicit solution approach can accurately describe the dynamic battery behaviors at a low computational cost.

To validate the prediction performance of the proposed explicit solution approach, the constructed model is applied to predict the voltage responses for an unseen HPPC dataset at 313 K. Figures 8a, b show the comparison of prediction results using the best three-, six-, and eighteen-term models at the whole SOC and the 60–70% SOC, respectively. As expected in Figure 8a, the three-term model has the worst performance in predicting the battery voltage responses, with a RMSE of 17.62 mV and a MAPE of 0.41%. The other two models with larger MC show the similar performance and both can accurately predict the battery voltage responses especially at high and medium SOC. For the entire SOC range, the RMSE values of the six- and eighteen-term models are 13.03 and 12.52 mV, respectively, and the MAPE of them are 0.30% and 0.28%, respectively. If neglecting the low SOC region below 30%, the RMSE values of the six- and eighteen-term models are decreased to 10.79 and 11.02 mV, respectively, and both MAPEs are reduced to 0.24%. It indicates that the model prediction error at low SOC region is larger than that at both medium and high SOC regions. The main reason is that the OCV model at low SOC region usually has larger prediction error than that at higher SOC region. Compared to the fitting results in Figure 7a, it is also found that the prediction error is about two times larger than the fitting error. That is mainly due to the fact that the model, only constructed from the voltage response curves during low-rate constant discharge-rest period, usually results in large prediction error for high-rate discharge processes in HPPC condition. In addition, HPPC test includes rest-charge voltage response processes, which might show a different dynamic behavior from discharge-rest processes. However, it should be pointed that the model with a prediction RMSE of about 13 mV is sufficiently low for practical system-level application. Moreover, it is expected that the prediction performance of the model can be further improved through introducing various voltage response curves for parameter estimation. From the enlarged section at the 60–70% SOC shown in Figure 8b, it is easy to see that the three-term model fails to accurately predict the exponential change regions during the all periods, while both the six- and eighteen-term models can almost perfectly capture the nonlinear dynamic behaviors. It indicates that the best six-term model is complex enough to replace a complete polynomial model for performing battery voltage response prediction in the relatively complex operating conditions. Hence, the

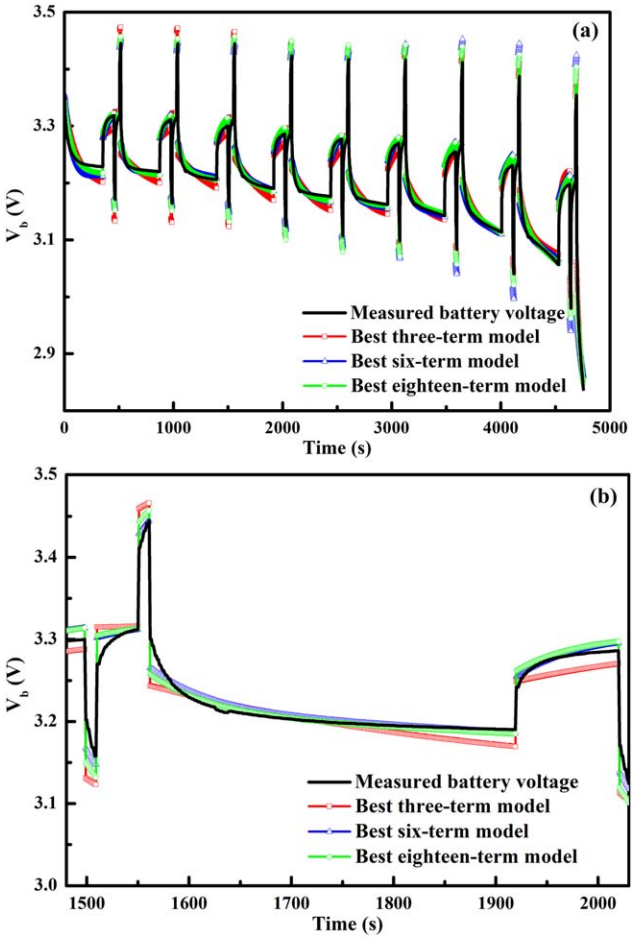

Figure 8. Comparison of prediction results of battery voltage responses using the three-, six-, and eighteen-term models in HPPC test at 313 K: (a) 0–100% SOC; (b) 60–70% SOC.

[Color figure can be viewed in the online issue, which is available at wileyonlinelibrary.com.]

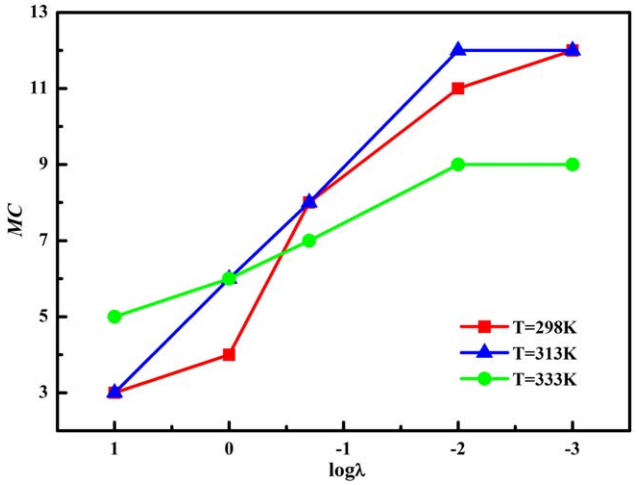

Figure 9. MC curves with respect to logλ under different temperatures in PCD test.

[Color figure can be viewed in the online issue, which is available at wileyonlinelibrary.com.]

effectiveness of the explicit solution approach is again demonstrated and the best model obtained from the explicit solution approach has the superior performance in terms of the trade-off between the model accuracy and complexity.

Model validation using the implicit solution approach

The implicit solution approach is used to construct the ECM model using PCD test at different temperatures. The MINLP models **P2** are sequentially solved for five prescribed regularization parameters, namely log$\lambda = 1$, 0, -0.6, -2, and -3. Figure 9 plots the model complexity MC with respect to the logarithm of regularization parameter under 298, 313, and 333 K. As shown in Figure 9, the value of MC usually increases with the decreasing of regularization parameter at a specific temperature. Generally, with the decreasing of the regularization parameter, the fitting accuracy term in the objective MINLP model **P2** could become dominated. Hence, a more complex model can be constructed by reducing the regularization parameter. Unlike the explicit solution approach, the implicit solution approach cannot guarantee to find all possible optimal models with all MCs without proper selection of the sequentially changed regularization parameter. For example, at the temperature of 313 K, the value of MC could suddenly change from to 3 to 6 as the logλ changes from 1 to 0. It indicates that the value of logλ should be properly selected between [0, 1] for obtaining the models with MCs of 4 and 5. If the value of regularization parameter sequentially decreases with a very small step for covering all possible solutions, the computational cost would significantly increases. Hence, a series of regularization parameter should be properly prescribed in advance for practical applications.

Figures 10a, b show the fitting RMSE and MAPE with respect to logλ at 298, 313, and 333 K, respectively. Similar as Figures 5a, b, the fitting error at low temperature is larger than that at high temperature. It indicates that the model is usually relatively difficult to fit the voltage response curve with sharp changes at low temperature. Compared to the values of RMSE and MAPE for a same MC in Figures 5a, b, it is found that the implicit solution approach often has larger fitting error, especially for a low MC value. For example, the RMSE and MAPE are 51.2 mV and 1.21% for a MC of 3 at 298 K, respectively, while the corresponding RMSE and MAPE are only 15.4 mV and 0.40% using the explicit solution approach, respectively. That is mainly caused by the inclusion the model complexity penalty in the objective function of MINLP model **P2**, which would make the implicit approach difficult to find a better solution, especially in case of relatively large regularization parameter. However, it is also observed that when the value of logλ decreases below 0, the fitting error of the implicit approach would become almost the same as that of the explicit approach for three temperatures. Both RMSE and MAPE values first decrease with the decreasing of logλ and then keep constant as the value of logλ below 0. From Figures 10a, b, both RMSE and MAPE curves have the logλ turning points of -0.6, 0, and 0 at the temperatures of 298, 313, and 333 K, respectively. The corresponding model complexity MCs are 8, 6, and 6. It further illustrates that a relatively simple model can be used to fit the battery voltage response behavior at high temperature.

The criterion C is calculated to assist multicriteria decision making and Figure 11 plots the criterion C with respect to logλ at 298, 313, and 333 K. Similar as Figure 6, for all three temperatures, the value of C usually first increases and then decreases with the decreasing of logλ. A larger value of C often corresponds to a better optimal solution for balancing

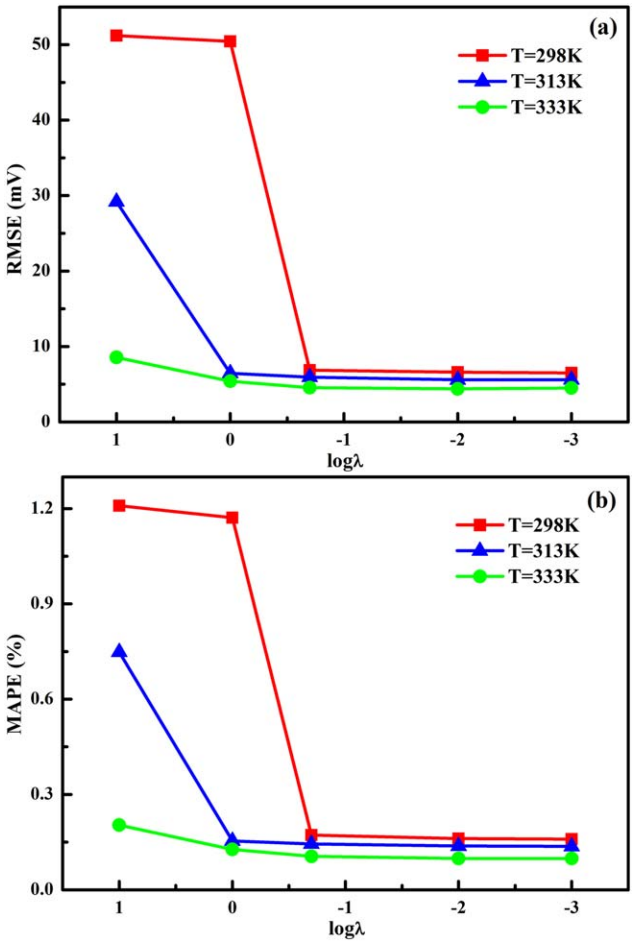

Figure 10. Model fitting performance with respect to logλ at different temperatures in PCD condition using the implicit solution approach: (a) RMSE; (b) MAPE.

[Color figure can be viewed in the online issue, which is available at wileyonlinelibrary.com.]

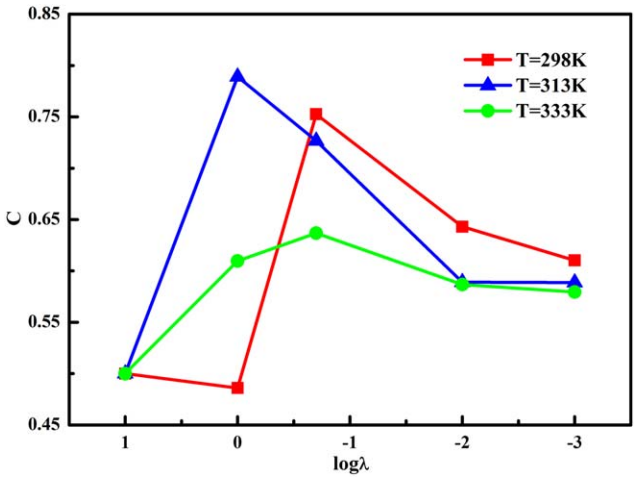

Figure 11. Criterion of model with different logλ under different temperatures in PCD test.

[Color figure can be viewed in the online issue, which is available at wileyonlinelibrary.com.]

the model accuracy and complexity. It is found that the maximum values of C are achieved with the logλ values of -0.6, 0, and -0.6 at 298, 313, and 333 K, respectively. The corresponding models have eight, six, and seven terms at 298, 313, and 333 K, respectively. Compared to the explicit approach, the implicit approach would construct slight complex models at 298 and 333 K. The main reason is that the determination of ideal and nadir ideal solutions in the explicit is different from that in the implicit approaches.

Figure 12 compares the fitting results of battery voltage responses using the models obtained with log$\lambda = 1$, 0, and -3 in PCD test at 313 K. The corresponding models have three, six, and twelve terms. Figure 12a shows that the fitting battery voltage responses obtained from the three-term model with log$\lambda = 1$ poorly match the measured data over the entire SOC range. It is found that the three-term model would significantly underestimate and overestimate the battery voltages at high and low SOC regions, respectively. The RMSE and MAPE of the three-term model are 29.2 mV and 0.69%, respectively. The six- and twelve-term models obtained with logλ values of 0 and -3 can match very well with the measured data over the entire SOC range. The RMSE values of the six- and twelve-term models are only 6.46 and 5.60 mV, respectively, and the MAPE values of them are 0.16% and 0.14%, respectively. From the enlarged section at the 60–70% SOC shown in Figure 12b, it can be clearly seen that the three-term model almost displays a linear characteristic and fails to capture the nonlinear characteristic of the battery in both discharge and rest periods, while the six- and twelve-term models could perfectly capture the nonlinear voltage response in the discharge period and exhibit a relatively small overestimation of terminal voltage in the rest period. As the six-term model has a comparable fitting performance with a more complex twelve-term model, the effectiveness of the implicit approach is thus demonstrated.

The prediction performance of the implicit solution approach is also validated by means of applying the above constructed three models to predict the voltage responses for an unseen HPPC dataset at 313 K. Figures 13a, b show the comparison of prediction results using the models obtained with log$\lambda = 1$, 0, and -3 at whole SOC and the 60–70% SOC, respectively. Figure 13a indicates that the three-term model obtained with log$\lambda = 1$ has the worst prediction performance, with a RMSE of 37.46 mV and a MAPE of 0.87%. The six-term model obtained with log$\lambda = 0$ has almost comparable prediction performance with the twelve-term model obtained with log$\lambda = -3$. The RMSE values of six- and twelve-term models are 15.12 and 13.30 mV, respectively, and the MAPE values of them are 0.35% and 0.31%, respectively. If neglecting the low SOC region below 30%, the RMSE values of six- and twelve-term models are decreased to 10.24 and 10.10 mV, respectively, and the MAPE values of them are reduced to 0.23% and 0.21%, respectively. Similarly to the prediction results in the explicit approach, the implicit approach also performs worse prediction performance at low SOC region, which might be caused by the inaccuracy of OCV model at low SOC region. Moreover, the prediction error is significantly larger than the fitting error, which is mainly caused by the operating modes of HPPC test is different from that of the PCD test for model construction. As mentioned in the explicit approach, the accuracy of the model can be further improved by the inclusion of various voltage response curves for parameter estimation. The enlarged section at the 60–70% SOC shows that, the three-term model almost represents a step response and fails to capture the battery nonlinear characteristics, while the other two models can accurately track the battery dynamic

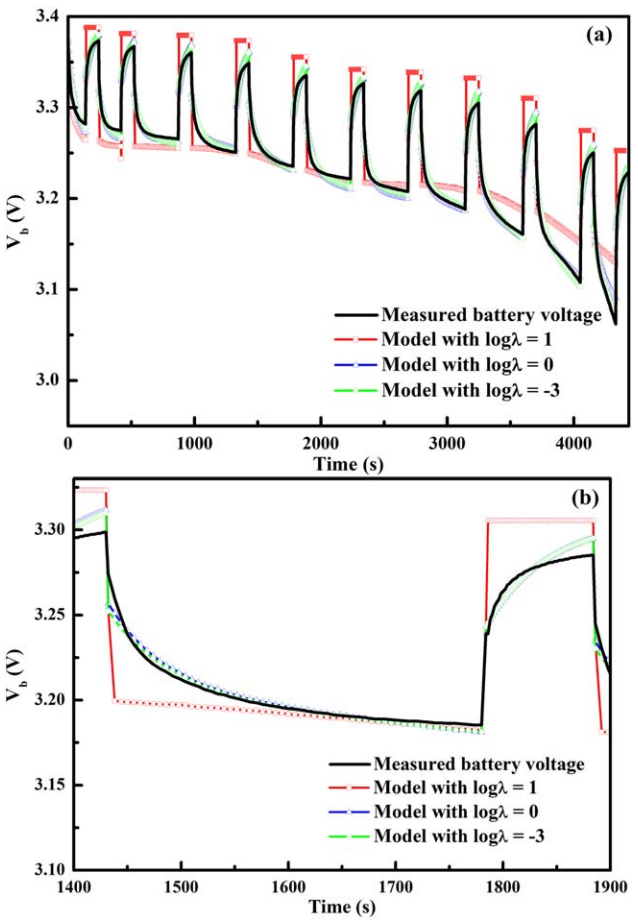

Figure 12. Comparison of fitting results of battery voltage responses using the models obtained with log $\lambda = 1$, 0, and -3 in PCD test at 313 K: (a) 0–100% SOC; (b) 60–70% SOC.

[Color figure can be viewed in the online issue, which is available at wileyonlinelibrary.com.]

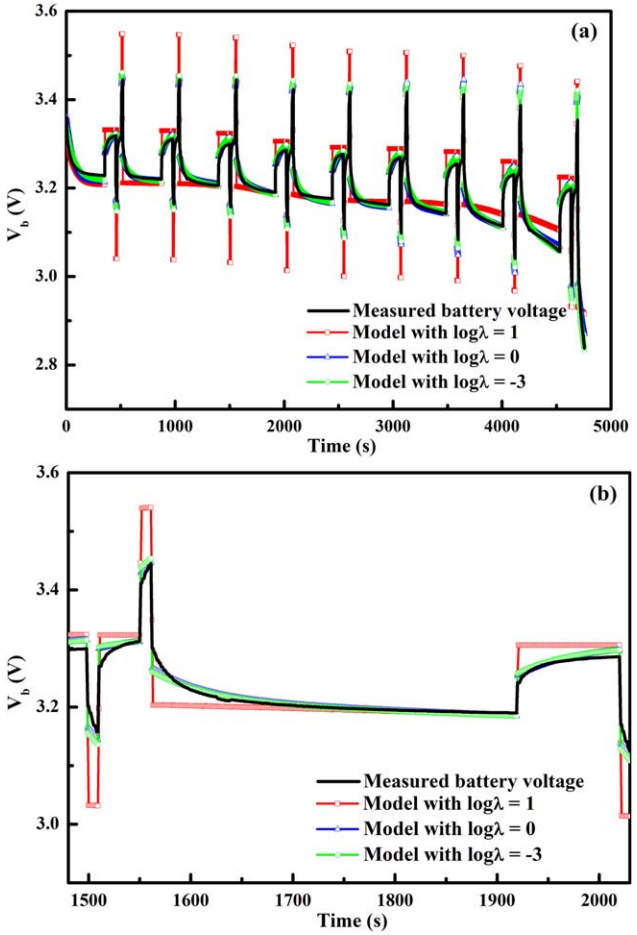

Figure 13. Comparison of prediction results of battery voltage responses using the models obtained with log $\lambda = 1$, 0, and -3 in HPPC test at 313 K: (a) 0–100% SOC; (b) 60–70% SOC.

[Color figure can be viewed in the online issue, which is available at wileyonlinelibrary.com.]

behaviors. The comparable prediction performance between six- and twelve-term models further indicates that a simple model can be effectively obtained using the implicit approach to replace a more complex model, which is helpful to improve computational efficiency in practical applications such as SOC estimation and SOH monitoring.

Some notes on the explicit and implicit solution approaches

The fitting and prediction results illustrate that both the explicit and implicit approach could find a satisfactory model with the trade-off between the model accuracy and complexity. It is found that the constructed model using the explicit approach is different from that using the implicit approach. Moreover, the fitting and prediction performance of the explicit approach is better than that of the implicit approach. In practical real-time applications such as SOC estimation and SOH monitoring, the constructed ECM by both approaches can meet the precision requirement. However, the explicit approach could theoretically and practically guarantee the iterative evaluation of all possible combinations of functional forms in ECM by means of simply increasing the model complexity MC value one by one until the termination criterion are met. Conversely, the implicit approach should properly prescribe a series of regularization parameters in advance; otherwise some possible optimal solutions corresponding to different model complexities would be omitted. Hence, compared to the implicit approach, the explicit approach is much easier to use in practice.

Based on the complexity analysis of MINLP models **P1** and **P2**, it is found that although the model **P2** is a little more complex than the model **P1** in terms of the number of variables and constraints, the computational time of model **P2** using BARON are faster than that of model **P1**. In practice, both explicit and implicit approaches only need to sequentially solve several MINLP models when use the proposed multicriteria decision making-based stopping criterion. The ECM is usually established in an offline way and needs to be online update using state/parameter estimation methods such as Kalman filtering and particle filtering for SOC estimation and SOH monitoring. Although the computational cost would be increased during the offline model construction procedure when using the proposed explicit and implicit approaches, a model with minimum complexity can be obtained, which would be greatly helpful to improve the computational efficiency for the online SOC estimation and SOH monitoring. Meanwhile, the proposed methods are implemented in an automatic way and rarely need to be intervened by the user, which could avoid empirically determining the proper functional forms using the trial-and-error method.

Conclusions

A systematical solution framework is proposed for simultaneous functional form selection and parameter estimation in ECM of LIBs. A bi-objective MINLP model is constructed by simultaneously optimizing two conflicting objectives, namely the model accuracy and model complexity. Then, two solution approaches are developed to tackle the bi-objective MINLP model. The explicit approach treats the objective of model complexity as an additional constraint, while the implicit approach replaces this objective with an l_1 norm penalty on polynomial coefficients. The transformed MINLP model is finally sequentially solved using BARON for both approaches, in which an ideal and nadir ideal solutions-based criterion is utilized to terminate the solution procedure for determining the optimal functional forms. Both PCD and HPPC tests at different temperatures of a commercial LIB are used to validate the effectiveness of the explicit and implicit approaches.

For both explicit and implicit approaches, the fitting error first decreases with the increasing of model complexity and then keeps almost constant. For a relatively simple optimal ECM with less than eight terms, the fitting RMSE and MAPE are less than 7 mV and 0.20% in PCD test, respectively, and the corresponding prediction RMSE and MAPE are also less than 15 mV and 0.25% in HPPC test, respectively. The fitting voltage response curves in PCD test and the prediction curves in HPPC test illustrate that the obtained optimal ECM could almost accurately capture the nonlinear dynamic behaviors of LIBs in discharge, charge, and rest periods. The outstanding fitting and prediction performance indicate that the proposed methods can effectively construct an optimal ECM with minimum complexity and prescribed precision requirement, which could be greatly helpful toward efficient and accurate SOC estimation and SOH monitoring.

Acknowledgments

The authors gratefully acknowledge financial support from the Major State Basic Research Development Program of China

(2014CB239703), the National Natural Science Foundation of China (21576163, 21006084, 21336003), the Science and Technology Commission of Shanghai Municipality (14DZ2250800), and the Project-sponsored by SRF for ROCS, SEM.

Literature Cited

1. Gao DW, Mi C, Emadi A. Modeling and simulation of electric and hybrid vehicles. *Proceedings of the IEEE*. 2007;95:729–745.
2. Jongerden MR, Haverkort BR. Which battery model to use? *IET Softw*. 2009;3:445–457.
3. Rao R, Vrudhula S, Rakhmatov DN. Battery modeling for energy-aware system design. *Computer*. 2003;36:77–87.
4. Pattipati B, Sankavaram C, Pattipati KR. System identification and estimation framework for pivotal automotive battery management system characteristics. *IEEE Trans Syst Man Cybern C Appl Rev*. 2011;41:869–884.
5. Cheng KWE, Divakar BP, Wu H, Ding K, Ho HF. Battery-management system (BMS) and SOC development for electrical vehicles. *IEEE Trans Veh Technol*. 2011;60:76–88.
6. Ng J, Dubljevic S. Boundary control synthesis for a lithium-ion battery thermal regulation problem. *AIChE J*. 2013;59:3782–3796.
7. Seaman A, Dao TS, McPhee J. A survey of mathematics-based equivalent-circuit and electrochemical battery models for hybrid and electric vehicle simulation. *J Power Sources*. 2014;256:410–423.
8. Doyle M, Fuller TF, Newman J. Modeling of galvanostatic charge and discharge of the lithium polymer insertion cell. *J Electrochem Soc*. 1993;140:1526–1533.
9. Chen M, Rincon-Mora GA. Accurate electrical battery model capable of predicting runtime and I–V performance. *IEEE Trans Energy Convers*. 2006;21:504–511.
10. Hariharan KS, Senthil Kumar V. A nonlinear equivalent circuit model for lithium ion cells. *J Power Sources*. 2013;222:210–217.
11. Moss PL, Au G, Plichta EJ, Zheng JP. An electrical circuit for modeling the dynamic response of Li-ion polymer batteries. *J Electrochem Soc*. 2008;155:A986–A994.
12. Chiasserini CF, Rao RR. Improving battery performance by using traffic shaping techniques. *IEEE J Sel Areas Commun*. 2001;19:1385–1394.
13. Chiasserini CF, Rao RR. Energy efficient battery management. *IEEE J Sel Areas Commun*. 2001;19:1235–1245.
14. Jang J, Yoo J. Equivalent circuit evaluation method of lithium polymer battery using Bode plot and numerical analysis. *IEEE Trans Energy Convers*. 2011;26:290–298.
15. Fleischer C, Waag W, Heyn H-M, Sauer DU. On-line adaptive battery impedance parameter and state estimation considering physical principles in reduced order equivalent circuit battery models. *J Power Sources*. 2014;260:276–291.
16. Buller S, Thele M, DeDoncker RWAA, Karden E. Impedance-based simulation models of supercapacitors and Li-ion batteries for power electronic applications. *IEEE Trans Ind Appl*. 2005;41:742–747.
17. Zhang JC, Ci S, Sharif H, Alahmad M. An enhanced circuit-based model for single-cell battery. In: *2010 Twenty-Fifth Annual IEEE Applied Power Electronics Conference and Exposition*. Palm Springs, CA: IEEE Press, 2010:672–675.
18. Malik A, Zhang Z, Agarwal RK. Extraction of battery parameters using a multi-objective genetic algorithm with a non-linear circuit model. *J Power Sources*. 2014;259:76−786.
19. Kroeze RC, Krein PT. Electrical battery model for use in dynamic electric vehicle simulations. In: *2008 IEEE Power Electronics Specialists Conference*. Rhodes, Greece: IEEE Press, 2008:1336–1342.
20. Kim T, Qiao W. A hybrid battery model capable of capturing dynamic circuit characteristics and nonlinear capacity effects. *IEEE Trans Energy Convers*. 2011;26:1172–1180.
21. Hu TS, Zanchi B, Zhao JP. Simple analytical method for determining parameters of discharging batteries. *IEEE Trans Energy Convers*. 2011;26:787–798.
22. Hu Y, Yurkovich S, Guezennec Y, Yurkovich BJ. Electro-thermal battery model identification for automotive applications. *J Power Sources*. 2011;196:449–457.
23. Erdinc O, Vural B, Uzunoglu M. A dynamic lithium-ion battery model considering the effects of temperature and capacity fading. In: *2009 International Conference on Clean Electrical Power*. Capri, Italy: IEEE Press, 2009:374–377.
24. Baronti F, Fantechi G, Leonardi E, Roncella R, Saletti R. Enhanced model for lithium-polymer cells including temperature effects. In: *IECON 2010 - 36th Annual Conference on IEEE Industrial Electronics Society*. Glendale, AZ: IEEE, 2010:2329–2333.
25. Hu X, Li S, Peng H. A comparative study of equivalent circuit models for Li-ion batteries. *J Power Sources*. 2012;198:359–367.
26. Zhang HL, Chow MY. Comprehensive dynamic battery modeling for PHEV applications. In: *2010 IEEE Power and Energy Society General Meeting*. Minneapolis, MN: IEEE Press, 2010:1–6.
27. Hentunen A, Lehmuspelto T, Suomela J. Time-domain parameter extraction method for Thevenin-equivalent circuit battery models. *IEEE Trans Energy Convers*. 2014;29:558–566.
28. Tawarmalani M, Sahinidis NV. A polyhedral branch-and-cut approach to global optimization. *Math Program*. 2005;103:225–249.
29. He YJ, Shen JN, Shen JF, Ma ZF. Embedding monotonicity in the construction of polynomial open-circuit voltage model for lithium-ion batteries. A semi-infinite programming formulation approach. *Ind Eng Chem Res*. 2015;54:3167–3174.
30. Hu XS, Li SB, Peng H, Sun FC. Charging time and loss optimization for LiNMC and $LiFePO_4$ batteries based on equivalent circuit models. *J Power Sources*. 2013;239:449–457.
31. Miranda AG, Hong CW. Integrated modeling for the cyclic behavior of high power Li-ion batteries under extended operating conditions. *Appl Energy*. 2013;111:681–689.
32. Hunt G, Motloch C. FreedomCAR battery test manual for power-assist hybrid electric vehicles. In: DOE/ID-11069. INEEL, Idaho Falls, USA, 2003.

Manuscript received June 3, 2015, and revision received Aug. 26, 2015.